Journal of Materials Chemistry C

PAPER

View Article Online
View Journal | View Issue

Cite this: J. Mater. Chem. C, 2014, 2, 9196

The impact of orbital hybridization on the electronic structure of crystalline InGaZnO: a new perspective on the compositional dependence

Youngho Kang,[a] Sanghyun Lee,[b] Hasung Sim,[bc] Chang Hee Sohn,[bc] Won Goo Park,[b] Seul Ji Song,[d] Un Ki Kim,[d] Cheol Seong Hwang,[d] Seungwu Han*[a] and Deok-Yong Cho*[bce]

Received 14th July 2014
Accepted 11th September 2014

DOI: 10.1039/c4tc01529k

www.rsc.org/MaterialsC

We report an investigation of the electronic structure of crystalline InGaZnO (IGZO) using X-ray absorption spectroscopy (XAS) and *ab initio* density functional theory calculations. The electronic properties of the conduction band vary significantly with the composition of $InGaZnO_4$ and $In_2Ga_2ZnO_7$, and this is strongly correlated with the XAS spectra. Detailed analyses of the orbital character reveal crystal field splitting under characteristic local structural distortions of the ZnO_5 coordinate bonds, which breaks the In p/d orbital degeneracy and preferentially lowers the energies of the In p_z and d($3z^2 - r^2$, xz/yz) orbitals near the Zn ions. The In s–p/d orbitals hybridize and contribute to the low-energy features of the In 5s orbitals. Therefore, the strong dependence of the electronic structure on the composition can be understood in terms of the abundance of distorted ZnO_5 coordination near the In^{3+} ions. In the case of amorphous IGZO, however, the XAS study and the *ab initio* calculations consistently show that the dependence of the electronic structure on the composition is significantly weaker than it is for crystalline IGZO, which is due to the lack of distinct symmetry in the s–p/d mixed orbitals. This work demonstrates that orbital hybridization is significant in determining the detailed low-energy electronic structure of crystalline IGZO.

I. Introduction

There has been significant effort in developing alternatives to amorphous Si (a-Si) for thin-film transistors (TFTs) used in next-generation liquid-crystal displays (LCDs) and organic light-emitting diode (OLED) displays.[1–7] The most promising materials are oxide semiconductors, which typically contain post-transition metal elements, such as Zn, Ga, Sn, or In. Correspondingly, the highly electronegative cations are capable of determining the electronic properties, which can lead to electrical behavior that is superior to that of a-Si. Indium gallium zinc oxide (IGZO) has attracted much research interest because of the high electron mobility ($\sim$10 $cm^2\ V^{-1}\ s^{-1}$) in amorphous IGZO (a-IGZO), which is one of the most significant features of merit for applications in flexible and/or large-area transparent devices.[5,8–10]

The favorable electrical properties of a-IGZO result from the dispersive and isotropic nature of the 5s orbitals in the In^{3+} ions, which are electron donors.[8,11] However, a-IGZO has fundamental issues in terms of stability in response to external stress. The device performance may vary significantly following the application of a bias[12–14] or illumination with ultraviolet (UV) or visible light;[15–18] it is expected that the vulnerability of the soft material is responsible for this degradation.[19,20] The softness of the bonds and consequent formation of deep defect levels in the amorphous material may result in undesirable effects, such as temperature bias illumination instability.[21,22] Crystalline IGZO (c-IGZO) may be superior to a-IGZO in terms of stability at the expense of losing the flexibility and uniformity at the atomic scale due to the presence of grain boundaries. Indeed, Sharp recently developed an LCD panel for iPads based on (partially) crystalline IGZO rather than a-IGZO.[23] It is therefore important to understand the electronic structure of c-IGZO to facilitate further improvement of the electrical properties of TFTs.

In spite of the growing importance of c-IGZO, most fundamental studies of IGZO have focused on the amorphous system only. This may be because a-IGZO is easier to fabricate at or near room temperature by sputtering. The electrical properties of a-IGZO vary depending on the composition of the cations,[24,25]

[a]Department of Materials Science and Engineering and Research Institute of Advanced Materials, Seoul National University, Seoul 151-755, Korea. E-mail: hansw@snu.ac.kr
[b]Center for Correlated Electron Systems, Institute for Basic Science (IBS), Seoul National University, Seoul 151-747, Korea
[c]Department of Physics & Astronomy, Seoul National University, Seoul 151-747, Korea
[d]Department of Materials Science and Engineering, Inter-University Semiconductor Research Center, Seoul National University, Seoul 151-744, Korea
[e]Department of Physics, Chonbuk National University, Jeonju 561-756, Korea. E-mail: zax@jbnu.ac.kr

and each cation appears to play a role in determining the electrical properties. For example, an abundance of Ga results in a low carrier concentration because of the high oxygen binding energy, which is essential for use as a semiconductor; however, it also results in low electron mobility.[26] It is generally accepted that a large In content results in a high n-type carrier concentration and high electron mobility because of the large overlap of the In 5s orbitals.[8,10,11] However, IGZO containing a very large In fraction becomes metallic.[27] The role of Zn remains unclear, but it has been argued that it may stabilize the amorphous structure with its preference for tetrahedral coordination.

In this work, we study the electrical properties of c-IGZO, considering the influence of the crystal symmetry on the electrical properties of c-IGZO, in particular, the electronic structure of the conduction band (CB), since the majority of carriers in IGZO are electrons. We examine the electronic structure of the CB of c-IGZO composed of In : Ga : Zn = 1 : 1 : 1 ($InGaZnO_4$) and 2 : 2 : 1 ($In_2Ga_2ZnO_7$). The orbital-resolved local density of states (DOS) of the CB is obtained both theoretically using density functional theory (DFT) calculations, and experimentally using X-ray absorption spectroscopy (XAS). We investigate the significance of the orbital hybridization on the CB structure and the dependence on the composition of the material. We show that the In 5s orbital states near the CB minima are strongly hybridized with the In 5p and 5d orbitals, preferentially along the *c*-axis of IGZO, which depends critically on the Zn concentration near the In ions. The amorphous counterparts of a-$InGaZnO_4$ and a-$In_2Ga_2ZnO_7$ are also employed in order to highlight the influence of the structural relaxation.

II. Methods

A. Density functional theory

The DFT calculations[28,29] of crystalline $InGaZnO_4$ and $In_2Ga_2ZnO_7$ were performed using the Vienna *Ab inito* Simulation Package (VASP) with projector-augmented wave (PAW) pseudopotential.[30,31] The PBEsol functional[32] was employed to calculate the exchange correlation energy, and the remaining computational parameters were the same as those in ref. 33. The 500 eV of cutoff energy for plane wave basis and the $7 \times 7 \times 1$ *k*-point mesh grid for Brillouin zone integration were employed for both compositions. Here, the calculated cells contained 3 In, 3 Ga, 3 Zn, and 12 O atoms for $InGaZnO_4$ and 4 In, 4 Ga, 2 Zn, and 14 O atoms for $In_2Ga_2ZnO_7$. The calculated values of the lattice constants were $a = 3.32$ Å and $c = 25.78$ Å for trigonal $InGaZnO_4$ ($R\bar{3}m$), and $a = 3.32$ Å and $c = 29.25$ Å for hexagonal $In_2Ga_2ZnO_7$ ($P6_3/mmc$), which is consistent with the results of the X-ray diffraction measurements (see Section III. A). Supercell calculations were carried out to simulate amorphous $InGaZnO_4$ and $In_2Ga_2ZnO_7$. To obtain the amorphous structures, we carried out first-principles molecular dynamics (MD) simulations. In order to generate the final amorphous structure more efficiently, we first determined the cubic supercell with the gravimetric density 2–5% smaller than that of the crystalline phase, and then, randomly distributed the atoms with certain constraints on the interatomic spacing, which allows

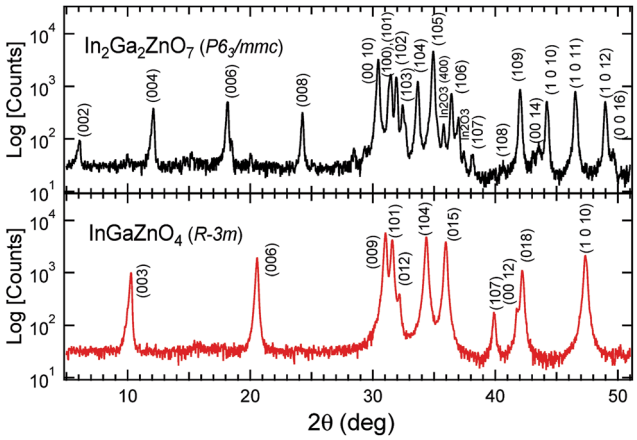

Fig. 1 XRD data for polycrystalline $InGaZnO_4$ and $In_2Ga_2ZnO_7$. The crystal symmetries determined by Rietveld refinement are $R\bar{3}m$ for $InGaZnO_4$ and $P6_3/mmc$ for $In_2Ga_2ZnO_7$. The lattice constants of $InGaZnO_4$ are $a = 3.30$ Å and $c = 26.00$ Å, while those of $In_2Ga_2ZnO_7$ are $a = 3.31$ Å and $c = 29.42$ Å. The numbers in parentheses show the reflectance (*hkl*) indices.

shortening of the melting time. We built two different cubic supercells containing 16 and 10 formula units of $InGaZnO_4$ and $In_2Ga_2ZnO_7$, which were then heated at 2000 K for 5 ps and cooled quickly to 300 K at a rate of -300 K ps^{-1}. Amorphous structures were obtained by full relaxation of the cell volume and atomic positions.[34]

B. X-ray measurements

Polycrystalline $InGaZnO_4$ and $In_2Ga_2ZnO_7$ powders (Toshima Manufacturing Inc.) were used for the X-ray measurements. The crystallinity of the powders was examined by X-ray diffraction (XRD) using a Miniflex II (Rigaku) diffractometer. The chemical properties of each of the ionic species in the IGZO system were investigated using X-ray photoelectron spectroscopy (XPS; see Fig. 2); it was confirmed that in both samples, the valences were

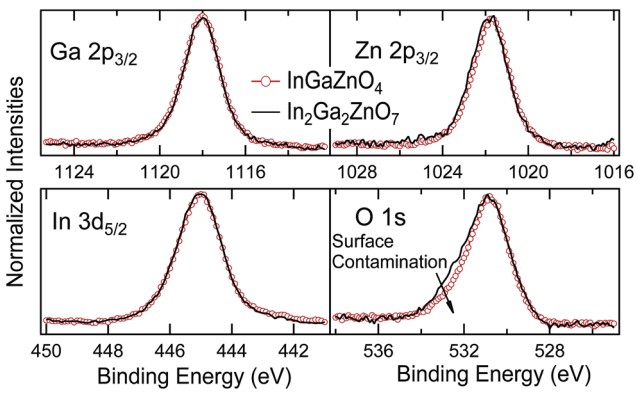

Fig. 2 Ga $2p_{3/2}$, Zn $2p_{3/2}$, In $3d_{5/2}$, and O 1s core level XPS spectra. For each of the core levels, the BEs of the $InGaZnO_4$ and $In_2Ga_2ZnO_7$ are almost the same with each other, reflecting the nearly identical chemistry. A small higher-BE shoulder in O 1s spectra originates from surface contamination.

In^{3+}, Ga^{3+}, Zn^{2+}, and O^{2-}. Soft X-ray absorption spectroscopy at the O K-, Ga L_3- and Zn L_3-edges was carried out using pelletized powder samples at the 2A beamline in the Pohang Light Source in total electron yield mode. For more details of the analyses of the Ga L_3-and Zn L_3-edge XAS spectra, see Section III. D.

III. Analysis and discussion

A. Characterization of the IGZO powders

Crystallinity. Fig. 1 shows X-ray diffraction (XRD) patterns of polycrystalline $InGaZnO_4$ and $In_2Ga_2ZnO_7$ powders. Each diffraction pattern was assigned according to the crystal symmetries of the respective systems, *i.e.*, $R\bar{3}m$ for $InGaZnO_4$ and $P6_3/mmc$ for $In_2Ga_2ZnO_7$. For $In_2Ga_2ZnO_7$, most of the XRD patterns can be assigned to the $P6_3/mmc$ phase, except for a small contribution (less than 5%) from a segregated phase of In_2O_3, whereas in the case of $InGaZnO_4$, all of the patterns may be attributed (almost perfectly) to a single $R\bar{3}m$ phase. This indicates that the powder samples were pure and crystalline. The lattice constants extracted from these data are $a = 3.30$ Å and $c = 26.00$ Å for $InGaZnO_4$ ($R\bar{3}m$), and $a = 3.31$ Å and $c = 29.42$ Å for $In_2Ga_2ZnO_7$ ($P6_3/mmc$), which are consistent with previous reports.[35]

Chemistry. The chemical properties of the In, Ga, Zn, and O ions were examined using the core level XPS. Samples were pelletized to minimize the contribution of surface effects. Fig. 2 shows normalized core level peaks for each of the ions. It is clear that the binding energies ($BE = E - E_F$; E_F is the Fermi level) of the core levels were almost identical for the two compositions. (The small high-BE-shoulder in the O 1s XPS spectra may be attributed to contamination by states at the surface of the pellet.) This indicates that the chemistry of all ionic species does not vary with the composition. In particular, the fact that O 1s BEs are identical in the two samples suggests that the significant variation of the O K-edge XAS data originates from structural variations, rather than differences in the chemistry of the O ions.

B. Crystal structure

Fig. 3a shows the crystal structure of $InGaZnO_4$ and $In_2Ga_2ZnO_7$ obtained from the DFT calculations following relaxation. In $InGaZnO_4$, two bipyramidal MO_5 clusters (where M is either Ga or Zn) are entangled to form a rigid $M_2O_{2.5}$ unit, leaving InO_6 to

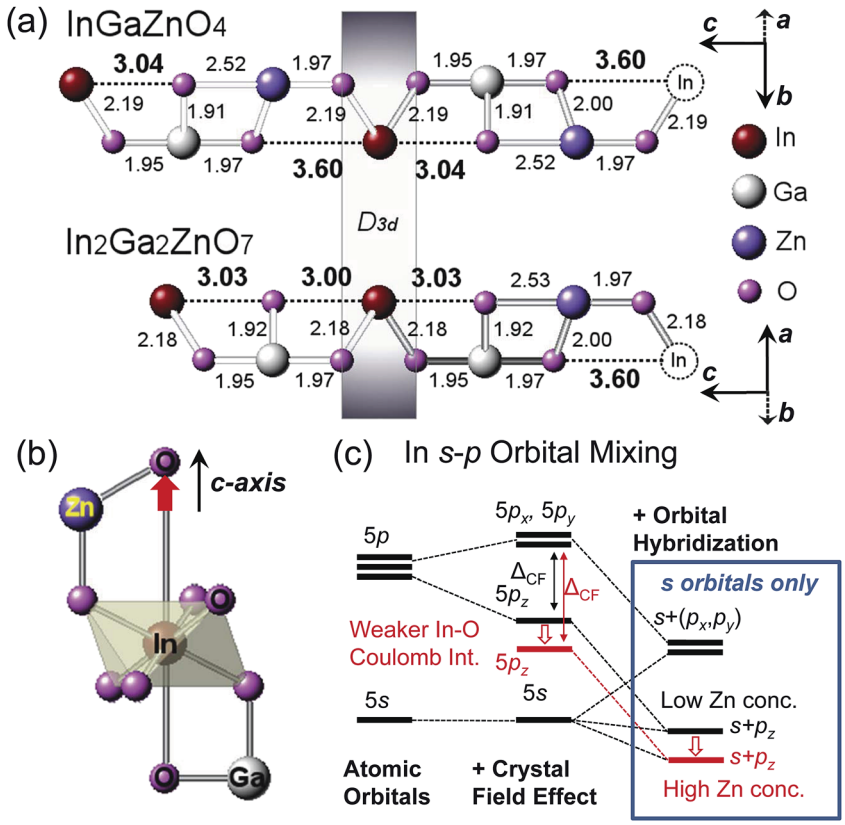

Fig. 3 (a) Results of the hybrid-functional calculations (PBEsol) for the crystal structures of $InGaZnO_4$ and $In_2Ga_2ZnO_7$. The numbers indicate the bond lengths in Å. Besides the octahedral coordination of the InO_6 cluster (D_{3d} symmetry), two longer In–O bonds exist along the *c*-axis (shown by the dotted lines). The ZnO_5 clusters are distorted to significantly elongate the additional In–O bonds nearby. (b) Atomic structure with structural distortions in the Zn–O coordination near the InO_6 cluster. The O ion at the highest position moves upwards due to distortion of the ZnO_5 cluster. This results in a reduction in the energies of the In orbitals along the *c*-axis. (c) Energy-level splitting caused by In s–pd hybridization in InO_6 (D_{3d}) + O_2. When the Zn concentration is large, the abundance of distorted ZnO_5 clusters near the In^{3+} ions results in a weakened Coulomb interaction and a lower energy of the hybridized states.

form an $InO_{1.5}$ unit and the stacking sequence of the In atom along the *c*-axis is the same as the [111] direction of the face-centered-cubic structure (ABCABC…), which leads to the formation of a unit cell in rhombohedral symmetry ($R\bar{3}m$). In $In_2Ga_2ZnO_7$, only two out of the three MO_5 clusters are mixed, and one MO_5 remains as a $MO_{1.5}$ unit constituting a unit cell of hexagonal symmetry ($P6_3/mmc$).[36] These structures agree well with the present XRD experiments and previous studies on the structure of such compounds.[36–38] There are several ways to arrange Ga and Zn atoms in the $M_2O_{2.5}$ or $MO_{1.5}$ units. In order to find an energetically favorable arrangement among them, we analyzed some of the structural features of the c-IGZO considered in the previous theoretical and experimental studies, and compared the energies between those competing structures.

It is found that there exist two important features in the detailed structures of the IGZO system. One is the arrangement of the Ga/Zn atoms in the $M_2O_{2.5}$ units sandwiched between the $InO_{1.5}$ units as shown in Fig. 3a. We modeled several equivalent structures of $InGaZnO_4$ and performed DFT calculations to examine which configuration is the most stable. Fig. 3a shows the reference structure wherein both the Ga and Zn "planes" (the atomic layers perpendicular to the *c*-axis) appear in the same $M_2O_{2.5}$ unit and they alternate along the *c*-axis. This reference structure ($GaZnO_{2.5}$) can be compared to a case where each $M_2O_{2.5}$ unit can include either Ga or Zn atoms separately (as in an alternating array of $Ga_2O_{2.5}$ + $Zn_2O_{2.5}$). Our test calculation showed that the energy of the reference model is 100 meV per atom lower than the case of the separate occupation. It is found that in the latter case there exists an in-plane strain on both Ga and Zn layers due to the difference between the bond lengths in the Ga- and Zn-containing clusters. This results in a significant increase of energy. Therefore, it is favorable to mix the Ga and Zn atoms within the same $M_2O_{2.5}$ unit.

Meanwhile, the occupation of the Ga/Zn atoms can also alternate along the *a*- or *b*-axis. This is also modeled with a $2 \times 1 \times 1$ supercell in which Ga and Zn atoms form stripe patterns when viewed from the *c*-axis. This structure was found to have almost the same but slightly lower energy (by only 10 meV per atom), suggesting no clear preference in the lateral alternations within the $M_2O_{2.5}$ unit. This is consistent with the experimental finding of random distribution of the Ga/Zn atoms in $InGaZnO_4$.[1] This cation disorder was found to play a critical role in limiting the electron mobility in c-IGZOs.[39,40] However, it was reported that when the composition of Zn is much higher than that of Ga, some ordered structures appear and Ga atoms are modulated in a zigzag shape between the $InO_{1.5}$ units.[41]

In a previous study of Da Silva *et al.* (ref. 42), the local structures of the $M_2O_{2.5}$ units were explained in terms of the inversion domain boundary (IDB) that connects the reversed polarity of the oxygen tetrahedra between neighboring InO layers. According to IDB theory, only Ga atoms can form IDB with the fivefold bipyramidal configuration because Ga atoms have more valence electrons than Zn atoms. A switching test, in which the Ga and Zn atoms are replaced by each other, resulted in an energy increase of ~200 meV per atom, indeed showing the stability of the ordered structure.

The second characteristic feature in the structure is that in the case of $In_2Ga_2ZnO_7$ with $P6_3/mmc$ symmetry, the $MO_{1.5}$ units should be introduced being compatible with the hexagonal symmetry (see Fig. 3a). Since a metal atom in the $MO_{1.5}$ unit is connected with oxygen atoms in the above and below $InO_{1.5}$ layers, its local structure forms the trigonal bipyramid and at the same time constitutes the IDB. This suggests that the Ga atoms should occupy primarily the $MO_{1.5}$ units rather than $M_2O_{2.5}$ units and the local structure of Ga in the $MO_{1.5}$ unit should appear to be the same with that in the $M_2O_{2.5}$ unit, in both $InGaZnO_4$ and $In_2Ga_2ZnO_7$. We also performed a switching test in which the Ga atoms in the $MO_{1.5}$ unit and the Zn atoms in the $M_2O_{2.5}$ unit are interchanged and found that the energy increases by 230 meV per atom. This again suggests the reliability of our reference model structure.

All the results of the aforementioned tests strongly suggested that the simple reference structure shown in Fig. 3a is an appreciably stable configuration. Therefore, we utilized the reference structures to evaluate the structure effect in the IGZO system. And we examine the mixing effects of Ga/Zn sites by employing the $3 \times 3 \times 1$ supercells of $InGaZnO_4$ and $In_2Ga_2ZnO_7$, distributing the Ga and Zn atoms randomly in $M_2O_{2.5}$ units (while distributing the Ga atoms only in $MO_{1.5}$ units for the case of $In_2Ga_2ZnO_7$).

We observed that the angle between the Ga–O bonds both along and perpendicular to the *c*-axis was almost 90°. This suggests that the GaO_5 clusters were not distorted in either $InGaZnO_4$ or $In_2Ga_2ZnO_7$. The structural rigidity remained whether the Ga^{3+} ions occupied the $M_2O_{2.5}$ or the $MO_{1.5}$ unit forming the IDB. The length of each bond is numerated in Fig. 3a. All the Ga–O bond lengths were close to 2 Å (1.91 Å to 1.97 Å; see Fig. 3a). However, the ZnO_5 clusters were significantly distorted with an O_A–Zn–O_P angle of 106° for both systems (where O_A denotes apical and O_P in-plane oxygen atoms). This instability of the bipyramidal local structure (contrary to the case of the Ga ions) may be caused by the complicated nature of the interactions of the shallow Zn 3d levels (where the binding energy is approximately −10 eV) with the Zn 4sp CB orbitals.[36] Four of the Zn–O bonds (three in-plane bonds and one apical bond) had similar or slightly larger lengths as the Ga–O bonds (Zn–O: 1.97–2.00 Å), while the remaining single Zn–O bond toward the GaO_5 cluster entangled within the $M_2O_{2.5}$ unit was elongated by approximately 30% (>2.5 Å). This structural distortion has an important consequence, which will be described shortly.

The InO_6 octahedral cluster ($InO_{1.5}$ unit) was trigonally distorted with almost the same In–O bond length of ~2.2 Å. Besides the six In–O bonds, there were two additional long In–O bonds along the *c*-axis (shown by the thick dashed lines in Fig. 3a). Although the two bonds were significantly longer than the six short In–O bonds, they may still contribute to the crystal fields on the In^{3+} ions. Hence, oxygen coordination of the In^{3+} ions should be regarded as effectively 6 + 2. As shown in Fig. 3a, the distortion of the ZnO_5 cluster results in an elongation of the long In–O bond (to 3.60 Å) pointing towards the Zn atom. The increase in the In–O bond length due to the ZnO_5 distortion was almost the same as the increase in the Zn–O bond length,

reflecting the dominant role of the ZnO_5 distortion in the change in the $[InO_6]O_2$ coordination. This elongation lowered the Coulomb interaction between the electrons at the O and In ions. Therefore, the energies of the In orbital states that participated in the long bonds were preferentially lowered.

Fig. 3b shows the $[InO_6]O_2$ coordination in the presence of the Ga^{3+} and/or Zn^{2+} ions nearby. By distorting the ZnO_5 cluster, the Zn^{2+} ions can attract the oxygen atom, which results in a longer In–O bond, so as to bring the oxygen ion away from the InO_6 cluster. Meanwhile, the Ga^{3+} ions do not induce such an elongation of the In–O bond. Thus, the average distance between the InO_6 cluster and the O^{2-} ion shared by the ZnO_5 should increase with increasing Zn population near the InO_6 cluster. The Zn population near the InO_6 cluster generally increased as a function of the Zn concentration. For instance, with a low Zn concentration, the nearest cations to the InO_6 cluster were mostly Ga^{3+}, so the average InO_6–O bond length along the *c*-axis was shorter. Conversely, with a high Zn concentration, the nearest cations were mostly Zn^{2+}, so that the average InO_6–O length along the *c*-axis was longer. In addition, the Ga-rich phase has more $MO_{1.5}$ units (M is mostly Ga), which might hinder such distortion of the InO clusters. Therefore, a high Zn concentration will result in a lower average InO_6–O bond length.

It is found that in the random-mixed configuration, the bond angles of O–Ga(Zn)–O and the bond length are not uniquely defined as in the ordered structures. However, the elongation of the average InO_6–O bond length under Zn-rich conditions (in this case, $InGaZnO_4$) is clearly observed (not shown). This suggests that random mixing does not devaluate the effects of the local structural distortions.

The influence of the local structure on the electronic structure is shown schematically in Fig. 3c. Here, only s–p hybridization is shown for clarity, although s–d hybridization is also significant. If it were not for the additional two long In–O bonds, the InO_6 coordination would possess D_{3d} point group symmetry under trigonal crystal fields. A trigonal crystal field splits the triply degenerate p levels into p_x/p_y doublets and a p_z singlet.[43] The d orbital states are spilt into three states of an a_{1g} singlet ($3z^2 - r^2$), an e_g^1 doublet, and an e_g^2 doublet with increasing energy (not shown in the figure). When the lengths of the additional two In–O bonds increased, the Coulomb potential decreased at the In^{3+} site along the *c*-axis so that the p/d orbitals aligned along the *c*-axis (*i.e.*, p_z, $3z^2 - r^2$, and *xz*/*yz* levels, where the *z* direction is parallel to the *c*-axis) and were slightly reduced in energy (see the center part of Fig. 3c). In other words, the symmetry of the orbital configuration was lost when the In–O bond increased in length due to a high Zn concentration near the In^{3+} ions.

It appears that the arrangement of the orbitals in energy was not particularly important to the actual electrical properties, since thermal carrier generation occurred mostly at the low-lying In 5s orbital states. However, the In 5s orbital had a complex electronic structure, which was mixed with the p/d orbitals. From molecular orbital theory,[44] we may expect a strong mixing effect among the s and p/d orbitals in the O coordinated cluster. For example, the In^{3+} ions can have sp^3d^2 hybridized orbital states under the crystal field of an octahedral O coordination. Since the hybridized states possess a relatively localized and directional p/d character, they should be sensitive to the details of the local coordination.

In particular, the low-energy part of the In 5s structure is dominated by strongly hybridized s–p /d orbitals. The right-hand side of Fig. 3c shows the energy order of the hybridized s–p orbital states and the evolution thereof in response to changes in the atomic composition. Here, only the in-phase s–p hybridized states ($|s\rangle + |p\rangle$), which have mainly the s orbital character, are shown for clarity. The levels of the out-of-phase hybridized states ($|s\rangle - |p\rangle$) should exist at higher energies, and the s–d mixing effect is expected to be similar. The diagram clearly shows that the energy of the CB minimum (In 5s) can be lowered by increasing the Zn concentration. This tendency was observed in both the experimental and theoretical data.

C. Conduction band structure

Fig. 4a shows the O K-edge XAS spectra of the polycrystalline $InGaZnO_4$ and $In_2Ga_2ZnO_7$ powders. The features of the O K-edge ($h\nu$ ~530 eV) are primarily attributed to empty O 2p states. Therefore, as shown in Fig. 4b, the spectra can fit the theoretical O 2p DOS if the effect of core-hole creation is neglected. Since the O 2p states can be empty only through orbital hybridization with the cations, the orbital states of these cations should be also taken into account in order to understand the features. Our XPS data (Fig. 2) showed no difference in the chemistry of each ion between the two powders. Thus, we may also exclude the possibility of a chemical shift in the XAS. Furthermore, it is well known that in the case of O K-edge XAS, the core-hole effect is minimal because the core-hole is created in the O 1s state rather than the cation core orbitals, so the effect on the final state electron configuration of the cations is negligible. Thus, we can determine the O K-edge XAS as an experimental probe for the local DOS (LDOS) of the cations.

The most important finding from the data shown Fig. 4a is that compared with $InGaZnO_4$, a noticeable enhancement of the peak labeled B and a suppression of the peak labeled A was observed in the $In_2Ga_2ZnO_7$ spectrum. It follows that there were more empty states in the low-energy region of $InGaZnO_4$. The O 2p DOSs for $InGaZnO_4$ and $In_2Ga_2ZnO_7$ are shown in Fig. 4b; the dependence of these peaks on the composition was quite consistent with those in the experimental spectra. In particular, compared with the $In_2Ga_2ZnO_7$ LDOS, feature A in the $InGaZnO_4$ LDOS was shifted to a lower energy by approximately 0.5 eV, and the intensity of feature B was reduced. This may explain the drastic spectral evolution in features A and B observed in Fig. 4a.

To assign the features of the O 2p DOS, the In 5s, 5p, and 5d DOSs and the Ga/Zn 4s DOSs are displayed in Fig. 4c and d, respectively. The In 5s DOS had a narrow bandwidth, which predominantly contributed to the low-energy (<5 eV) features. The low-energy features (A and B) shown in Fig. 4b are very similar to those in the In 5s DOS, which suggests that the CB features resulted primarily from the In 5s orbitals. Feature C was dominated by Ga/Zn 4s DOS, and features D and E

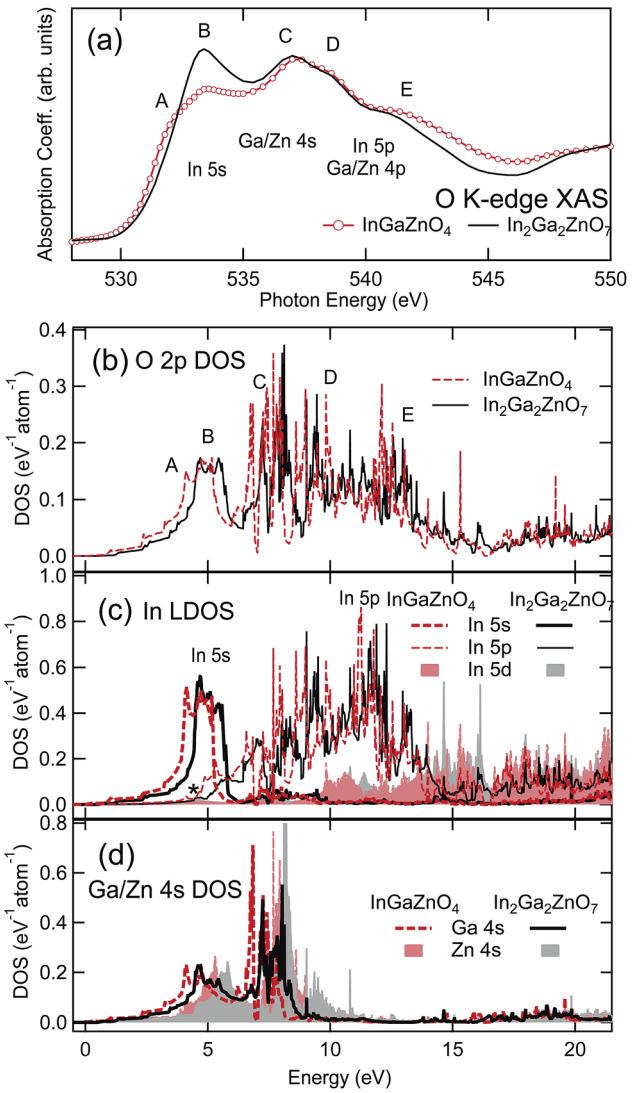

Fig. 4 (a) O K-edge XAS spectra. Calculated DOSs for (b) O 2p, (c) In 5s, 5p, and 5d, and (d) Ga 4s and Zn 4s. The features of the peaks labeled A to E in the XAS spectra and their variation in response to changes in the composition are consistent with the results of the calculations.

originated from the In/Ga/Zn p orbital states. Note that a small amount of In p and In d DOSs was observed in the In 5s energy range, as shown by the asterisk in Fig. 4c. This reflects the s–p /d orbital mixing effect in the In ions. As will be shown in the following section, this orbital hybridization significantly alters the low-energy features of the CB, despite the weakness of the contributions to the 5s DOS.

D. Orbital hybridization

Here, we focus on understanding the microscopic origin of the compositional dependence, particularly near the CB minimum. It is well known that in both $InGaZnO_4$ and $In_2Ga_2ZnO_7$, the atomic arrangement can be decomposed into successive connections of the metallic ions mediated by oxygen ions, as shown in Fig. 3a. The oxygen coordination of $[InO_6]O_2$ has a D_{3d} trigonal distortion, and the MO_5 bipyramids (D_3) can have an M site that is shared by the Ga^{3+} and Zn^{2+} ions. Ga^{3+} and Zn^{2+} ions have the same number of electrons and similar ionic radii, so they can occupy the same crystallographic site. Hence, it is often presumed that the two ions are randomly distributed over the M sites.[1,36]

However, even though the two ionic species can mix, it is not clear whether the local structures of GaO_5 and ZnO_5 clusters are identical. The local symmetry of an oxygen-coordinated metal ion cluster is determined by the coordination number itself. This is a consequence of the repulsive coulombic interactions between negative charges on the oxygen ions. Therefore, both GaO_5 and ZnO_5 clusters in $InGaZnO_4$ and $In_2Ga_2ZnO_7$ have trigonal bipyramidal coordination, whereas InO_6 has octahedral coordination (with a D_{3d} trigonal distortion). However, the details of the local structure, such as the angle between the M–O bonds and the subtle elongation or contraction, are determined by the electronic configuration as well as by the chemical environment surrounding the clusters.

Fig. 5a shows the Ga L_3-edge XAS spectra and Fig. 5b shows the Zn L_3-edge XAS spectra. These reflect the Ga/Zn 4s and 4d states modified by core-hole effects. To examine the electronic structure with the core-hole effect, XAS data were simulated using an *ab initio* real-space multiple scattering approach (*i.e.*, FEFF8), which is based on the model structure of $InGaZnO_4$. The simulated spectra reproduce the experimental spectra for both $InGaZnO_4$ and $In_2Ga_2ZnO_7$ accurately, suggesting the validity of the assignments of the features B–E in the O K-edge XAS spectra (Fig. 4a). Feature B may be attributed to the Ga/Zn 4s orbital states, whereas features C–E may be attributed to the Ga/Zn 4d orbital states. These d state features also appear in the O K-edge XAS spectra, since the d orbital states are also hybridized with O 2p states. Note that the intensity of the Ga 4s or Zn 4s states does not vary significantly with the composition in the experimental spectra. This indicates that the considerable differences in feature A in Fig. 4a cannot be explained by changes in the Ga or Zn LDOSs. Therefore, the suppression of

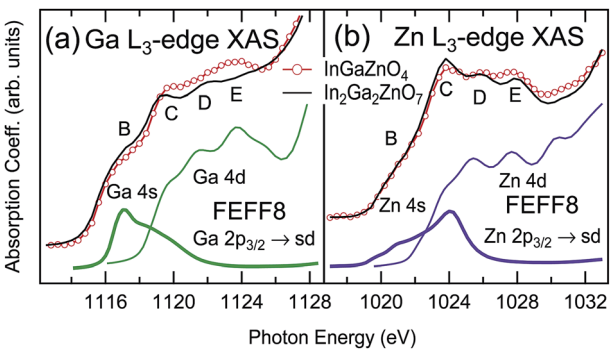

Fig. 5 (a) Ga L_3-edge and (b) Zn L_3-edge XAS spectra. The peaks are assigned B–E to be consistent with the data shown in Fig. 4a. The results of multiple scattering calculations (FEFF8) are also shown. The intensities of the Ga 4s and Zn 4s states barely change with the composition, suggesting that the emergence of feature A in Fig. 4a in the case of $InGaZnO_4$, does not originate from certain evolution in the Ga/Zn LDOS.

feature A in $In_2Ga_2ZnO_7$ compared with $InGaZnO_4$ suggests a strong sensitivity of the In 5s band structures to the local environment, which can be explained by a strong orbital mixing effect in the In ions.

As shown in Fig. 3, the calculated data show that a substantial distortion occurred in ZnO_5 but not in GaO_5, which could lower the energy of the s–p /d mixed orbitals in the nearby In^{3+} ions. The low-energy region of the LDOS revealed the effects of such local structural distortions. Fig. 6a–c (d–f) show the In, Ga, and Zn LDOSs of $InGaZnO_4$ ($In_2Ga_2ZnO_7$), respectively. All the energies were referenced to the values of the calculated electrostatic potentials. The LDOSs were normalized to the numbers of each cation to reflect the DOS per atom. Overall, the LDOSs of the $InGaZnO_4$ appeared to be similar to those of the $In_2Ga_2ZnO_7$ for each of the cations. We used the same nomenclature for features A to C as in Fig. 4. For both IGZO systems, the In 5s features were the most significant for the low-energy region, so they were primarily responsible for the electrical conduction through the empty states.[45] The Ga 4s features were dispersed over a wide energy range, whereas the Zn 4s features were more concentrated on feature B (at approximately +5 eV), consistent with the experimental findings in Fig. 5.

Note that there are several signatures of the CB tail states in In and Ga LDOS. It is known that these long tails are characteristics of the IGZO system, and strongly affect the electrical properties.[31] The energies of these tail states are approximately 1 eV lower in $InGaZnO_4$ than in $In_2Ga_2ZnO_7$. Because these tail states are part of the hybridized orbital states, they are related to the energy lowering in the high Zn concentration system ($InGaZnO_4$), as shown in Fig. 3c.

The DOSs of the p and d orbitals shown in Fig. 6 are magnified to highlight the contribution to the CB tails. It is clear that the p and d orbital states also exist near the minimum of the CB (at approximately +4 eV), although the DOSs were much smaller than those of the s orbitals. This reflects the orbital mixing through the sp^3d^2 hybridization in InO_6 and through the sp^3d hybridization in GaO_5 or ZnO_5 because otherwise, the p and d states would have significantly higher energies than the s states, as shown in Fig. 3c. Interestingly, the LDOSs of the five sub-shell states were very different from each other. As shown in the In LDOSs in Fig. 6a and d, only the $d(3z^2 - r^2)$ (a_{1g} symmetry) and p_z states were widely spread in energy, which contributes to the tail-like In 5s states, whereas the main In 5s features consisted mainly of other p and d orbitals. The dominance of the $d(3z^2 - r^2)$ or p_z in the tail-like states among the d or p orbitals suggests a low energy of the hybridized s–$d(3z^2 - r^2)$/ p_z states compared with other s–d/p subshell hybridized states.

In the Ga LDOS shown in Fig. 6b and e, the contribution of the $d(x^2 - y^2)/d(xy)$ and p_x/p_y became particularly strong in the features labeled A and B. This was because of the strong s–d/p orbital mixing in the plane of the oxygen triangle in the GaO_5 cluster, shown in the inset of Fig. 6b. As shown in the Zn LDOS in Fig. 6c and f, the contributions of $d(x^2 - y^2)/d(xy)$ and $p(x)/p(y)$ remained dominant; however, they were much weaker compared with those in the Ga LDOS. This could be attributed to a weaker s–$d(x^2 - y^2)/d(xy)$ or s–p_x/p_y mixing, due to the fact that the in-plane triangle in the ZnO_5 cluster was not in a centrosymmetric position (see the inset of Fig. 6c). Moreover, the features of the s–$d(3z^2 - r^2)$ hybridized states in the Zn LDOS

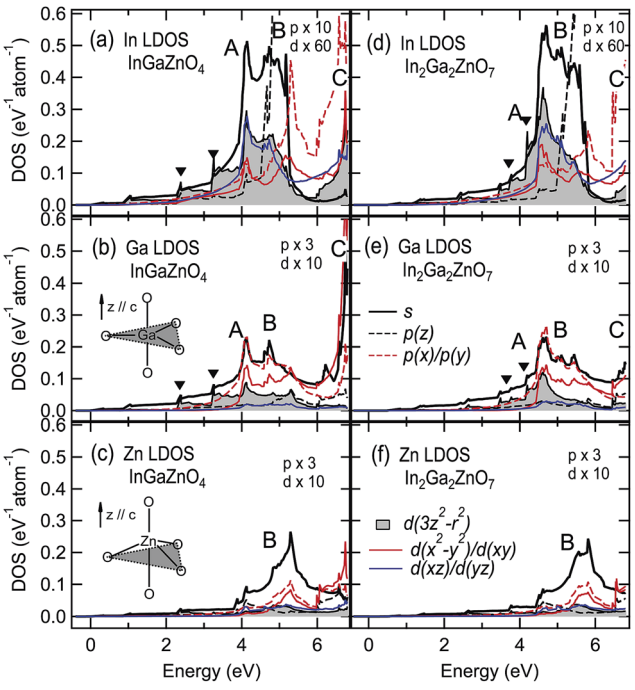

Fig. 6 LDOSs of the CB for (a–c) $InGaZnO_4$ and (d–f) $In_2Ga_2ZnO_7$. In 5s dominates the CB structure. A strong hybridization effect of the In s–p_z–$d(3z^2 - r^2)$ orbitals can be observed. The inset shows the undistorted (distorted) GaO_5 (ZnO_5) clusters. The signatures of the CB tail states in In and Ga LDOS are indicated by ▼ symbols in (a), (b), (d), and (e).

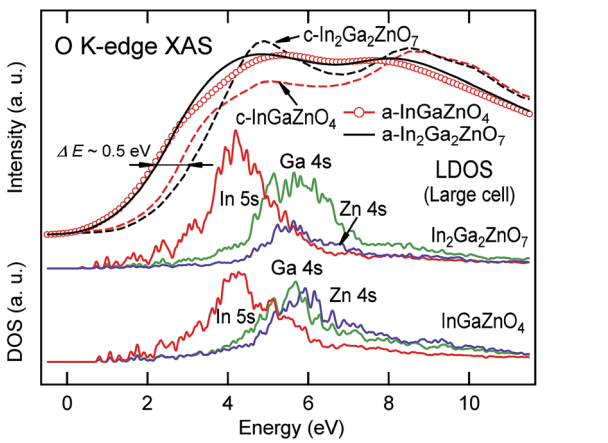

Fig. 7 O K-edge XAS data for amorphous $InGaZnO_4$ and $In_2Ga_2ZnO_7$ thin films (taken from ref. 36) as well as those for c-IGZO's, and the results of the calculations, showing the contrast between amorphous and crystalline IGZO. Compared with c-IGZO, the CB minimum of a-IGZO is lowered by approximately 0.5 eV, which is primarily due to a reduction of the energies of the main In 5s features, and this contributes to a reduction in the differences between the two compositions.

were weak compared with those of the Ga LDOS, suggesting the significance of the ZnO_5 distortion, and consequently resulting in a bond length change in the $[InO_6]O_2$ cluster.

E. Amorphous *versus* crystalline IGZO

Here, we compare the LDOS of c-IGZO with that of a-IGZO. Fig. 7 shows the O K-edge XAS data of *amorphous* $InGaZnO_4$ and $In_2Ga_2ZnO_7$ thin films (data taken from ref. 36) as well as the spectra of c-IGZOs. Overall, the changes in the spectra in response to variations in the composition (*i.e.*, $InGaZnO_4$ *versus* $In_2Ga_2ZnO_7$) were similar to those of the crystalline system (shown by the dashed lines in Fig. 7). However, the spectral changes were smaller than in the crystalline systems. Furthermore, the energies of the CB minimum were approximately 0.5 eV lower than those of the crystalline counterparts. The results of calculations using large cells to mimic the amorphous state of the model systems are appended to the same figure for comparison. The lowest energy features were dominated by the In 5s states. This was similar to c-IGZO; however, the contribution of the Ga 4s states, as well as of the Zn 4s states at the low-energy region (approximately +4 eV), was less significant than with crystalline IGZO.

Careful comparison of the LDOSs of c-IGZO (Fig. 6) and a-IGZO (Fig. 7) suggests that the main peaks of the In 5s (Ga/Zn 4s) orbitals indeed shifted to lower (higher) energies for both a-$InGaZnO_4$ and a-$In_2Ga_2ZnO_7$. The In 5s DOS separated out from the Ga/Zn 4s DOS suggests that the In 5s orbital can contribute to electrical conduction exclusively. It was also observed that the lower energy shift of the In 5s main peaks appeared to mitigate the contributions of the hybridized s–p/d states at energies around +4 eV. Therefore, the overall lower-energy shift of the In 5s main features made the electronic structures of the two amorphous systems much more similar to each other compared to those of the crystalline systems.

This insensitivity of the amorphous system to the composition is one of the advantages of a-IGZO for mass production, because it can lead to a weaker dependence on the deposition conditions. It has been demonstrated that the sensitivity of the electronic structure to the composition originates from s–p/d orbital hybridization in the In ions. If it were not for the orbital hybridization effect, the energies of In 5s orbitals would not be particularly sensitive to structural distortions because the s orbital itself is isotropic. The insensitivity has been regarded as one of the most important characteristics of transparent amorphous oxide semiconductors,[8,46] which is in stark contrast to the covalent nature of Si. In contrast, the orbital mixing effect becomes significant in c-IGZO due to the approximately 0.5 eV increase in energy of the main In 5s features. Therefore, orbital mixing should be taken into account when describing the electronic structure of crystalline or amorphous IGZO systems.

IV. Conclusion

We have theoretically and experimentally studied the electronic structure of crystalline and amorphous IGZO using DFT and X-ray spectroscopy methods. We found a sharp contrast in the electronic structure near the CB minima, depending on the composition of the amorphous and crystalline materials. In c-IGZO, the In 5s orbitals, which constitute the CB, were strongly hybridized with In p_z and $d(3z^2 - r^2)$ orbitals, so that the low-energy CB features were sensitive to local structural variations. Non-centrosymmetric distortion of the ZnO_5 coordination resulted in an elongation of the InO_6–O bonds along the *c*-axis, and consequently lowered the energy of the s–p_z/$d(3z^2 - r^2)$ mixed states. Therefore, the variation of the electronic structure in response to compositional changes could be explained by considering the distorted ZnO_5 near the In^{3+} ions. In a-IGZO, however, the main In 5s features occurred at energies that were lower by approximately 0.5 eV for both IGZO systems, which reduced the significance of orbital hybridization effects. It follows that orbital mixing should be considered for understanding the details of the low-energy electronic structure in c-IGZO systems.

Acknowledgements

This work was supported by the Research Center Program of the Institute for Basic Science (IBS), the Fundamental R&D Program for Core Technology of Materials, the Global Research Laboratory Program (2012040157) through the National Research Foundation of Korea, and the research funds of Chonbuk National University in 2014. The computations were carried out at the KISTI Supercomputing Center (KSC-2013-C3-039).

References

1 K. Nomura, H. Ohta, K. Ueda, T. Kamiya, M. Hirano and H. Hosono, *Science*, 2003, **300**, 1269.
2 T. Kamiya and H. Hosono, *NPG Asia Mater.*, 2010, **2**, 15.
3 K.-H. Lim, K. Kim, S. Kim, S. Y. Park, H. Kim and Y. S. Kim, *Adv. Mater.*, 2013, **25**, 2994.
4 M.-G. Kim, H. S. Kim, Y.-G. Ha, J. He, M. G. Kanatzidis, A. Facchetti and T. J. Marks, *J. Am. Chem. Soc.*, 2010, **132**, 10352.
5 S. Jeon, S.-E. Ahn, I. Song, C. J. Kim, U.-I. Chung, E. Lee, I. Yoo, A. Nathan, S. Lee, J. Robertson and K. Kim, *Nat. Mater.*, 2012, **11**, 301.
6 Y.-G. Lee and W.-S. Choi, *Electron. Mater. Lett.*, 2013, **9**, 719.
7 J. Y. Choi, S. Kim and S. Y. Lee, *Electron. Mater. Lett.*, 2013, **9**, 489.
8 K. Nomura, H. Ohta, A. Takagi, T. Kamiya, M. Hirano and H. Hosono, *Nature*, 2004, **432**, 488.
9 H. Yabuta, M. Sano, K. Abe, T. Aiba and T. Den, *Appl. Phys. Lett.*, 2006, **89**, 112123.
10 T. Kamiya, K. Nomura and H. Hosono, *J. Disp. Technol.*, 2009, **5**, 273.
11 A. Walsh, J. L. F. Da Silva and S.-H. Wei, *Chem. Mater.*, 2009, **21**, 5119.
12 J. Raja, K. Jang, N. Balaji, W. Choi, T. T. Trinh and J. Yi, *Appl. Phys. Lett.*, 2013, **102**, 083505.
13 M. D. H. Chowdhury, P. Migliorato and J. Jang, *Appl. Phys. Lett.*, 2011, **98**, 153511.
14 A. Suresh and J. F. Muth, *Appl. Phys. Lett.*, 2008, **92**, 033502.

15 H. Oh, S.-M. Yoon, M. K. Ryu, C.-S. Hwang, S. Yang and S.-H. K. Park, *Appl. Phys. Lett.*, 2010, **97**, 183502.
16 T. C. Chen, T. C. Chang, T. Y. Hsieh, C. T. Tsai, S. C. Chen, C. S. Lin, F. Y. Jian and M. Y. Tsai, *Thin Solid Films*, 2011, **520**, 1422.
17 K. H. Ji, J.-I. Kim, H. Y. Jung, S. Y. Park, R. Choi, U. K. Kim, C. S. Hwang, D. Lee, H. Hwang and J. K. Jeong, *Appl. Phys. Lett.*, 2011, **98**, 103509.
18 T.-C. Chen, T.-C. Chang, C.-T. Tsai, T.-Y. Hsieh, S.-C. Chen, C.-S. Lin, M.-C. Hung, C.-H. Tu, J.-J. Chang and P.-L. Chen, *Appl. Phys. Lett.*, 2010, **97**, 112104.
19 D.-Y. Cho, J. H. Kim, U. K. Kim, Y. J. Chung, J. Song, C. S. Hwang, J.-M. Lee and S.-J. Oh, *J. Phys. Chem. C*, 2010, **114**, 11962–11964.
20 D.-Y. Cho, J. Song and C. S. Hwang, *J. Phys. Chem. C*, 2009, **113**, 20463–20466.
21 B. Ryu, H.-K. Noh, E.-A. Choi and K. J. Chang, *Appl. Phys. Lett.*, 2010, **97**, 022108.
22 R. N. P. Vemuri, W. P. Mathews, M. Marrs and T. L. Alford, *J. Phys. D: Appl. Phys.*, 2013, **46**, 045101.
23 Y. Kataoka, H. Imai, Y. Nakata, T. Daitoh, T. M. N. Kimura, T. Nakano, Y. Mizuno, T. Oketani, M. Takahashi, T. I. Y. Hirakata, J. Koyama, S. Yamazaki, J. Koezuka and K. Okazaki, *SID Int. Symp. Dig. Tech. Pap.*, 2013, **44**, 771.
24 J.-Y. Huh, J.-H. Jeon, H.-H. Choe, K.-W. Lee, J.-H. Seo, M.-K. Ryu, S.-H. K. Park, C.-S. Hwang and W.-S. Cheong, *Thin Solid Films*, 2011, **519**, 6868.
25 K. Nomura, A. Takagi, T. Kamiya, H. Ohta, M. Hirano and H. Hosono, *Jpn. J. Appl. Phys.*, 2006, **45**, 4303.
26 H.-K. Noh, K. J. Chang, B. Ryu and W.-J. Lee, *Phys. Rev. B: Condens. Matter Mater. Phys.*, 2011, **84**, 115205.
27 H. Sim, S. Choi, J.-G. Park, J. Song, S. Han, C. S. Hwang and D.-Y. Cho, *ECS J. Solid State Sci. Technol.*, 2014, **3**, P10.
28 W. Kohn and L. J. Sham, *Phys. Rev.*, 1965, **140**, A1133.
29 P. Hohenberg and W. Kohn, *Phys. Rev.*, 1964, **136**, B864.
30 G. Kresse and J. Furthmüller, *Phys. Rev. B: Condens. Matter Mater. Phys.*, 1996, **52**, 11169.
31 G. Kresse and D. Joubert, *Phys. Rev. B: Condens. Matter Mater. Phys.*, 1999, **59**, 1758.
32 J. P. Perdew, A. Ruzsinszky, G. I. Csonka, O. A. Vydrov, G. E. Scuseria, L. A. Constantin, X. Zhou and K. Burke, *Phys. Rev. Lett.*, 2008, **100**, 136406.
33 Y. Kang, S. H. Jeon, Y. W. Son, Y. S. Lee, M. Ryu, S. Lee and S. Han, *Phys. Rev. Lett.*, 2012, **108**, 196404.
34 To confirm the validity of the present approach, we also carried out a reference calculation for $InGaZnO_4$ with 252 atoms in the unit supercell. The starting structure was a low-density crystalline structure and it was melted for 20 ps at 2000 K and cooled down to 300 K with a cooling rate of -300 K ps^{-1}. The final structure was confirmed to be very similar to that obtained with the method described in the text.
35 N. Kimizuka and T. Mohri, *J. Solid State Chem.*, 1995, **60**, 382.
36 D.-Y. Cho, J. Song, K. D. Na, C. S. Hwang, J. H. Jeong, J. K. Jeong and Y.-G. Mo, *Appl. Phys. Lett.*, 2009, **94**, 112112.
37 P. J. Cannard and R. J. D. Tilley, *J. Solid State Chem.*, 1998, **73**, 318.
38 L. Dupont, C. Maugy, N. Naghavi, C. Guery and J.-M. Tarascon, *J. Solid State Chem.*, 2001, **158**, 119.
39 K. Nomura, T. Kamiya, H. Ohta, K. Ueda, M. Hirano and H. Hosono, *Appl. Phys. Lett.*, 2004, **85**, 1993.
40 Y. Kang, Y. Cho and S. Han, *Appl. Phys. Lett.*, 2013, **102**, 152104.
41 C. Li, Y. Bando, M. Nakamura, M. Onoda and N. Kimizuka, *J. Solid State Chem.*, 1998, **139**, 347.
42 J. L. F. Da Silva, Y. Yan and S.-H. Wei, *Phys. Rev. Lett.*, 2008, **100**, 255501.
43 S. Sugano, Y. Tanabe and H. Kamimura, *Multiplets of Transition-Metal Ions in Crystals*, Academic Press, New York, 1980.
44 R. B. King, *J. Am. Chem. Soc.*, 1969, **91**, 7211.
45 D.-Y. Cho, J. Song, C. S. Hwang, W. S. Choi, T. W. Noh, J.-Y. Kim, H.-G. Lee, B.-G. Park, S.-Y. Cho, S.-J. Oh, J. H. Jeong, J. K. Jeong and Y.-G. Mo, *Thin Solid Films*, 2009, **518**, 1079–1081.
46 K. Nomura, T. Kamiya, H. Ohta, T. Uruga, M. Hirano and H. Hosono, *Phys. Rev. B: Condens. Matter Mater. Phys.*, 2007, **75**, 035212.

